Applied Materials Today 20 (2020) 100699

Contents lists available at ScienceDirect

Applied Materials Today

journal homepage: www.elsevier.com/locate/apmt

A flexible self-arched biosensor based on combination of piezoelectric and triboelectric effects

Yang Zou[a,d,1], Jingwen Liao[b,1], Han Ouyang[a,c], Dongjie Jiang[a,d], Chaochao Zhao[a,e], Zhe Li[a,d], Xuecheng Qu[a,d], Zhuo Liu[a,c], Yubo Fan[c], Bojing Shi[a,c,*], Li Zheng[b,*], Zhou Li[a,d,*]

[a] CAS Center for Excellence in Nanoscience, Beijing Key Laboratory of Micro-nano Energy and Sensor, Beijing Institute of Nanoenergy and Nanosystems, Chinese Academy of Sciences, Beijing 100083, China
[b] College of Mathematics and Physics, Shanghai Key Laboratory of Materials Protection and Advanced Materials in Electric Power, Shanghai University of Electric Power, Shanghai 200090, China
[c] Beijing Advanced Innovation Centre for Biomedical Engineering, Key Laboratory for Biomechanics and Mechanobiology of Ministry of Education, School of Biological Science and Medical Engineering, Beihang University, Beijing 100083, China
[d] School of Nanoscience and Technology, University of Chinese Academy of Sciences, Beijing 100049, China
[e] Department of Biomedical Engineering, School of Medical Engineering, Foshan University, Foshan 528000, China

ARTICLE INFO

Article history:
Received 28 February 2020
Revised 21 April 2020
Accepted 9 May 2020

Keywords:
Nanogenerator
Self-arched
Hybrid
Pulse sensor
Wearable

ABSTRACT

Wearable electronics bring convenience to our lives. Among them, flexible physiological sensors such as pulse sensors that can be used to monitor human health play critical roles. Recently, pulse sensors based on nanogenerators have received extensive attention in recent years, which have considerable properties including high sensitivity, signal-to-noise ratio and low power consumption due to their self-powered mode. Here, a self-powered pulse sensor based on a self-arched nanogenerator (SANG) with a combined effect of piezoelectric and triboelectric is demonstrated for real-time monitoring pulse waveform of the radial artery. The output properties of SANG are related to the morphology of the self-arched structure, which can be easily regulated by adjusting the mass ratio of two types of silicone elastomers of PDMS and Ecoflex. It is a convenient approach compared to conventional ones that should make a different special mold to obtain arched structures. For pulse sensing, the sensitivity and the stability of the SANG are qualified due to its unique self-arched structure and hybrid effect of triboelectric and piezoelectric for converting tiny mechanical signals into electric ones effectively.

1. Introduction

Real-time physiological monitoring plays a vital role in human convenient modern life [1–4]. It is becoming critical and indispensable for wearable electronics to contribute to the progression for biomedical applications, which may enhance the present level of the individual-centered disease diagnosis and healthcare [5–9]. Nanogenerators (NGs) that can convert mechanical energy into electricity are suitable for acting as sensors, especially to detect human physical signals such as sphygmus [10–13] According to the working principles, there are mainly two types of NGs: piezoelectric nanogenerators (PENGs) [14–18] and triboelectric nanogenerators (TENGs) [19–21]. PENGs are made by piezoelectric materials such as zinc oxide (ZnO) [22,23] lead zirconate titanate (PZT) [24,25] and poly (vinylidene fluoride) (PVDF) [26]. TENGs based on the combined effect of triboelectrification and electrostatic induction have developed rapidly due to the advantages of flexible, high sensitivity, self-powered and cost-effective [27–31]. In this work, we mainly focus on the TENG in vertical contact-separation mode, which has been widely used due to its good stability, flexibility, and versatility for many practical scenarios [32–34]. One of the basic structures of TENGs is a spacer to ensure contact-separation process working normally [35–37]. However, most spacer types of recent TENGs are gasket or spring, which may increase the difficulty of device fabrication and influence the stability and durability of the devices.

Here, we utilize the phenomenon of stress mismatch that occurs on the interface between two different polymer materials to fabricate a flexible self-arched structure which can replace spacer

* Corresponding authors.
E-mail addresses: bjshi@buaa.edu.cn (B. Shi), zhengli@shiep.edu.cn (L. Zheng), zli@binn.cas.cn (Z. Li).
[1] These authors contributed equally to this work.

https://doi.org/10.1016/j.apmt.2020.100699
2352-9407/

in conventional TENG devices. The self-arched structure also acts as one of the friction layers of TENG. Therefore, we demonstrate a self-arched nanogenerator (SANG) for pulse sensing, which takes advantage of the natural curvature caused by the stress mismatch existing at the interface of two silicone elastomer film materials. Meanwhile, to further improve the sensing performances, a PVDF film is introduced to be embedded into the self-arched structure of the SANG to form a hybrid nanogenerator based on the combined effect of triboelectricity and piezoelectricity, which can enhance the outputs, the signal-to-noise ratio and stability of the device when detecting pulse signals.

2. Material and methods

2.1. Preparation of self-arched polymer films

The self-arched polymer films were fabricated by a two-step method. The first step was to prepare a layer of cured Ecoflex film. Required amounts of parts A and B gel of Ecoflex silicone elastomer (Smooth-On, Ecoflex 00-10) were mixed in a container for 5 minutes (1A: 1B by volume or weight). The mixed gel of Ecoflex silicone elastomer was poured into a 1 cm × 3 cm mold, and a vacuuming operation was performed for 5 minutes to eliminate any entrapped air of mixture. Then, the mixture was cured at 50 °C for 4 hours to form a cured Ecoflex silicone elastomer film. The second step was prepared a layer of polydimethylsiloxane (PDMS) silicone elastomer onto the cured Ecoflex silicone elastomer layer. The gel of PDMS (Dow corning, Sylgard 184) was mixed thoroughly by the PDMS main agents and curing agents with a weight ratio of 10:1. Required amounts of the mixed gel of PDMS were weighed to make the mass ratio of PDMS/Ecoflex 3:2. After vacuumized for 30 minutes, the mixed gel of PDMS was poured into the mold placed with the prepared Ecoflex film. The whole sample was cured in an oven at 50°C for 4 hours. The self-arched structure was completed once the composite material of PDMS and Ecoflex was taken out from the mold. Finally, different self-arched polymer films were prepared by adjusting the mixture ratio of PDMS/curing agent (7:1, 5:1, 3:1) and the mass ratio of PDMS/Ecoflex (2:3, 2:1, 3:1).

2.2. Fabrication of SANG

The piezoelectric film used in this article is a commercial Metallized Piezo Film Sheets (Measurement Specialties, Inc., TE Connectivity company.). The PVDF membrane is coated with silver ink as electrodes on both sides and has been polarized. When used to assemble a piezoelectric nanogenerator, the piezo film sheet needs to be cut to the required size (1cm × 3cm), and the cut film needs to be scraped around to ensure that the electrodes on both sides are not conductive and cause a short circuit. Then, the two enameled copper wires were fixed to the electrodes on both sides of the piezo film with silver paste to prepare the piezoelectric element of the device. The piezoelectric element was placed on the PDMS side of the prepared self-arched film in the mold. A small amount of gel of PDMS was coated on the piezoelectric element and cured in an oven at 50°C for 4 hours. A self-arched film embedded a PENG was prepared after taking out from the mold. An aluminum foil (thickness, 25 μm) was cut into a size of 1 cm × 3 cm. The self-arched film was assembled with the Al foil to construct the triboelectric element of the device (by the Ecoflex side face to the Al foil). The junction of the self-arced film and Al foil was fixed by adhesive tape, and an enameled Cu wire was fixed on the Al foil by silver paste. Then a layer of PDMS was coated on the bottom of the Al foil to make the whole structure more stable. Finally, the prepared entire device was assembled with a woundplast for facilitating fit with the skin directly.

2.3. Characterization of SANG

The Fourier transform infrared (FTIR) results of the self-arched polymer film were characterized by the FTIR spectrometer (Bruker VERTEX80v). The mechanical properties of the SANG were tested by the force gauge (Mark-10 ESM303). The signals of SANG were measured by the electrometer (Keithley 6517B) and the oscilloscope (LeCroy HDO6104). The linear motor (LinMot E1100) was used to provide the periodic external force applied to the SANG. The images of the scanning electron microscope (SEM) were taken by Hitachi field emission SEM (SU8020).

3. Results and discussion

3.1. Structure, preparation and working principle of SANG

The SANG consists of a self-arched layer and a flat layer (Fig. 1a). The core part of the device is the self-arched structure, which is mainly caused by the residual stress gradient accumulated inside the composite materials during the curing stage (Fig. S1), and a thermal stress mismatch on the interface of the Ecoflex and the PDMS (Fig. 1b). The Ecoflex film in the self-arched layer and Al film in the flat layer form a triboelectric nanogenerator (TENG). The PVDF film with silver (Ag) electrodes is the core part of the piezoelectric nanogenerator (PENG). The whole device is fixed on a woundplast for sticking the SANG to the wrist more conveniently (Fig. 1c). Fig. 1d shows the mechanism of stress mismatch between PDMS and Ecoflex. The coefficient of thermal expansion (CTE) of PDMS is α_1 and that of Ecoflex is α_2. According to references [38–41], we know that α_1 (~ 266.5 ppm/°C) is larger than α_2 (~ 271.1 ppm/°C). When cooling, the different contractions between the PDMS and the Ecoflex lead to a bend to the Ecoflex side. At the same time, a residual stress gradient is accumulated inside the composite materials during the curing stage due to the restraining effect of the mould, which can further cause a large warpage of the sample after demoulding [42-45]. More explanation about the mechanism of composite materials forming a curved structure can be found in Supplementary Note 1. There, we only need simple operations of polymer film processing and device building to fabricate the SANG for pulse sensing (Fig. 1e and more details in the experimental section).

The layer details are demonstrated by a scanning electron microscope (SEM) image in Fig. 2a. From top to bottom, the layers are PDMS, PVDF, PDMS and Ecoflex, respectively. The corresponding thicknesses of each layer are 100 μm, 95 μm, 170 μm, 260 μm. To improve the triboelectric effect [46,47], some micropatterns were fabricated on the surface of the Ecoflex film through micromachining technology, as shown in the lower right corner of Fig. 2b. The width and height of micro-pyramid array structure are about 200 μm and 300 μm, respectively. The outermost layer of PDMS is an encapsulation layer (Fig. 2b). The molecular formula of PDMS and Ecoflex are similar so that the degree of crosslinking of these two materials can be very high, due to the tight connection of some radical groups on the interface of them (Fig. 2c). The results of Fourier transform infrared (FTIR) spectrometry measurements show that the PDMS and Ecoflex films have similar molecule groups. Therefore, the monomer of the Ecoflex easily penetrates in the PDMS at the interface and causes the molecular segment at the interface to be entangled after the polymerization (Fig. 2d).

The working process of the SANG is shown in Fig. 2e. At the initial state, the top arched layer is separated from the bottom layer. There is no piezoelectric and triboelectric potential in the device. When applying pressure on the SANG, the PVDF film in the arched layer is under a compressed strain, which will produce piezoelectric potential on the surfaces of it. At the same time, part of the silicone film in the arched layer contacts with the aluminum (Al)

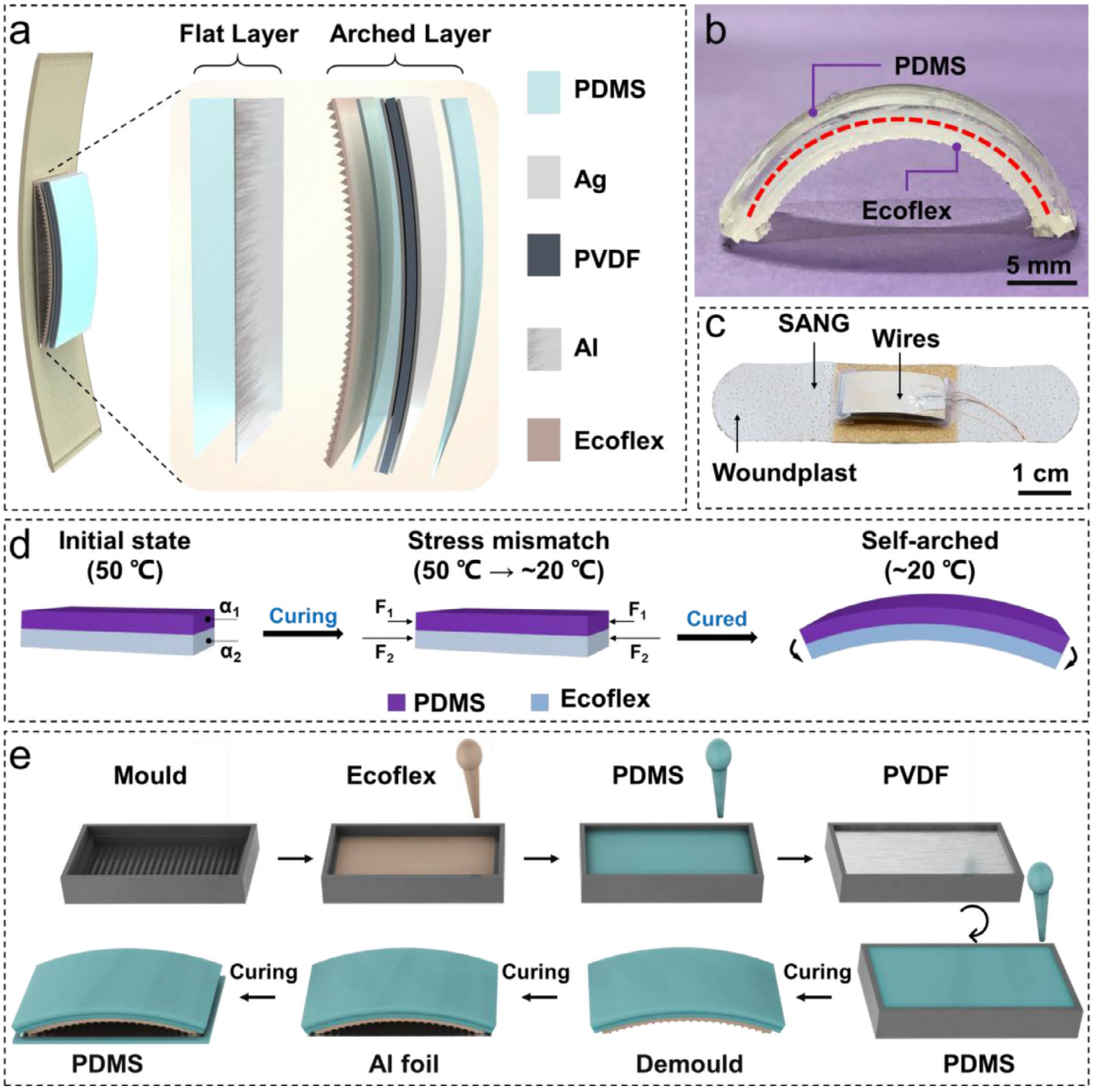

Fig. 1. (a) Schematic diagram of structure of SANG. (b) Photograph of self-arched structure of SANG. (c) Photograph of SANG. (d) Principle of thermal stress mismatch of the self-arched structure. The Ecoflex film has a larger contraction than PDMS when cooling from 50 °C to room temperature (~ 20 °C). (e) Schematic diagram of manufacturing process of SANG.

film of the bottom layer, resulting in charge transfer between the Ecoflex film and Al film due to triboelectric effect, which will form a potential difference between the Ag electrode on the Ecoflex film and the Al film. Till the top layer is contacted with the bottom layer fully, the piezoelectric and triboelectric potentials both reach the maximum. If connecting these electrodes by an external circuit, the current would appear during the deformation process of the SANG. Then the pressure is released, the SANG is recovering to the initial state, the electrons flow back from the Ag electrode to the Al electrode due to the potential difference decreasing according with the separation of the top and bottom layers, which causes a reverse current in the external circuit. The further working mechanism and the equivalent electrical circuit model of the PENG and TENG element of SANG are shown in Fig. S3 and Fig. S4, respectively. When applying a periodic force to the SANG continuously, a periodic signal of voltage and current can be detected. It is noteworthy that the triboelectric effect may not completely give contact electrification in some period of the test, which will include a certain of non-contact electrification like a freestanding mode of the TENG. The detailed process of the SANG working in freestanding mode is shown in Fig. S2.

3.2. Characterization of self-arched structure

Considering that the morphology of the self-arched structure of the SANG is related to the mixture ratio of PDMS/curing agent (MIR_{PC}) and mass ratio PDMS/Ecoflex (MAR_{PE}), we study the influences of MIR_{PC} and MAR_{PE} to the morphology of the self-arched structure quantitatively. Two experimental groups are prepared. The first one is Group A with MIR_{PC} of 5:1 and MAR_{PE} of 1:3, 1:2, 2:3, 3:2, respectively. The second is Group B with MAR_{PE} of 2:3 and MIR_{PC} of 10:1, 7:1, 5:1, 3:1, respectively. The morphologies of the self-arched structures of these two groups are shown in Fig. 3a and b. We have repeated the fabrications and tests of each group of samples five times, the corresponding bending degrees of each sample were measured and calculated separately. The average bending degree and standard deviation of each sample were acquired and presented as mean ± s.d. The results demonstrate that the bending degree of the self-arched structure was max when (MIR_{PC}, MAR_{PE}) is (5:1, 3:2) in Group A, and (3:1, 2:3) in Group B (Fig. 3d and e). It could be conjectured that stiffer and more PDMS might lead to a bigger camber of the self-arched structure.

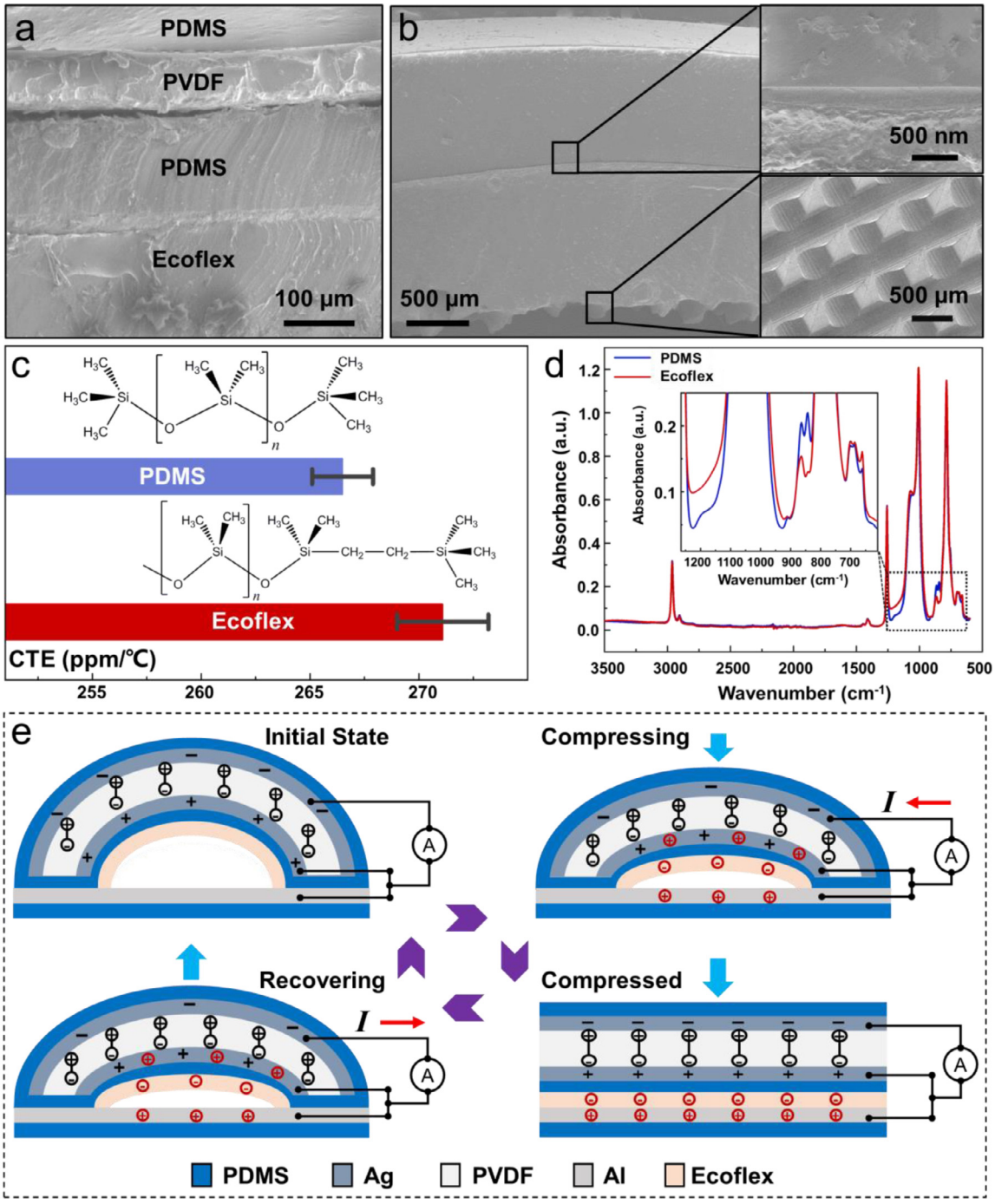

Fig. 2. (a) SEM image of sectional view of self-arched structure of SANG. (b) SEM images of sectional view of the self-arched structure and top view of Ecoflex surface with micro-patterns. (c) Molecular formula and coefficient of thermal expansion (CTE) of PDMS and Ecoflex. (d) Fourier transform infrared (FTIR) testing results of the interface of PDMS and Ecoflex. (e) Schematic diagram of working principle of SANG.

As Fig. 3f shown, the mechanical properties of the self-arched structure are studied. The sample is fixed to a platform then tested by force gauge. All samples of Group A and Group B are measured. In Group A, with the increase of the MAR_{PE}, the applied force increases gradually. When the MAR_{PE} is 3:2, the applied force is the largest under the same deformation of the self-arched structures. In Group B, as the MIR_{PC} increasing, the applied force is also increased. The relationship between the applied force (F) and deformation (D) of the self-arched structure is approximately linear within a certain range of deformations. The results of F/D are demonstrated in Fig. 3g. It can be got a conclusion that the self-arched structure with more ratio of PDMS needs larger external applied force. With different bending degrees, the device can work as a pulse sensor contacting the different complicated human skin and improve the sensibility. One of the noticeable advantages of the SANG is the self-arched structure that replaces the conventional spacer of this kind of device based on TENG. The elastic modulus of the self-arched structure is skin-like, which is softer and more comfortable to be attached to the wrist.

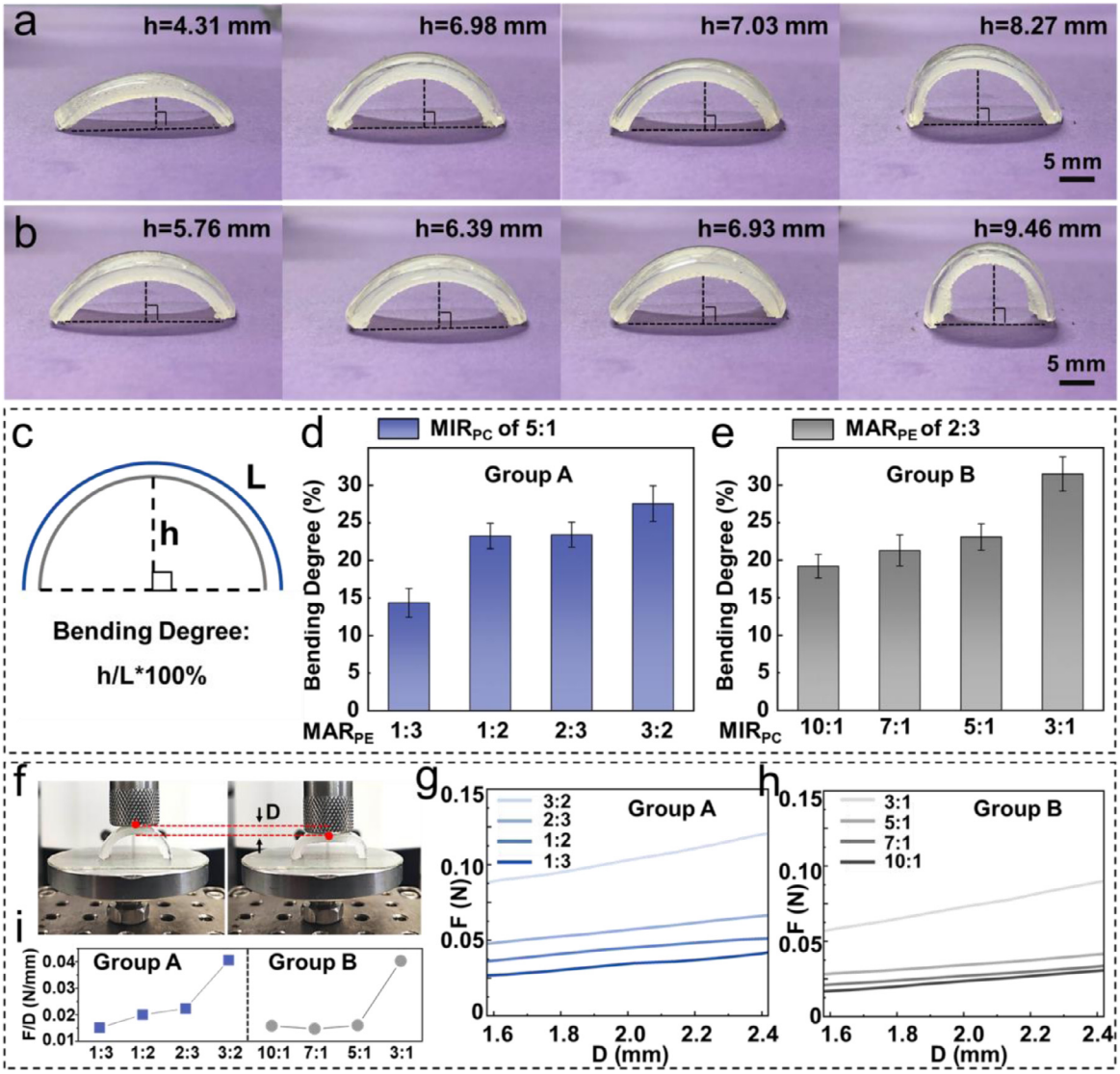

Fig. 3. (a) Morphologies of self-arched structures with same MIRPC and different MARPE (Group A). (b) Morphologies of self-arched structures with same MARPE and different MIRPC (Group B). (c) Definition of bending degree. (d) Bending degrees of samples in Group A. (e) Bending degrees of samples in Group B. (f) Mechanical test of self-arched structure. (g) Mechanical test results of samples in Group A. (h) Mechanical test results of samples in Group B. (i) Results of parameter of F/D.

3.3. Electrical performance of SANG

The output properties of triboelectric mode, piezoelectric mode, and hybrid mode of the SANG are shown in Fig. 4a–c. Open-circuit voltage (V_{oc}), short-circuit current (I_{sc}) and transferred charge quantity (Q) are measured under a periodic mechanical force with the triggering speed of 1 m/s^2 at the frequency of 1.2 Hz. The results show that the V_{oc} of triboelectric mode, piezoelectric mode and hybrid mode of the SANG are 6.5 V, 4.25 V and 5.2 V, respectively. Meanwhile, the I_{sc} and Q of these three modes of SANG have a significant difference. The I_{sc} of the hybrid mode of the SANG is about 500 nA, which is significantly higher than that of triboelectric mode (175 nA) and piezoelectric mode (250 nA). The trend of Q is similar to that of I_{sc}, which is 5.30 nC for hybrid mode, higher than that of triboelectric mode (2.51 nC) and piezoelectric mode (3.52 nC). When the piezoelectric element and triboelectric element of a SANG are connected in parallel, they together form an equivalent capacitance model, the equivalent electrical circuit model of a SANG is shown as Fig. S5. The equivalent model of the SANG and the basic rules are as follows:

$$Q = CV_{OC} \tag{1}$$

$$I_{SC} = \frac{\Delta Q}{\Delta t} \tag{2}$$

where C is the equivalent capacitance of different modes of the SANG. More explanation about the equivalent capacitance model of a SANG can be found in Supplementary Note 2. The results show that the output property of the hybrid mode of the SANG is superior to that of triboelectric and piezoelectric ones.

Fig. 4d reveals the relationship between the output properties of the SANG and applied external pressures. With different bending degrees, the relationship between the force and the voltage is different. Seven experimental groups are prepared and divide them into Group No.1 and Group No.2. The samples of SANG of Group No.1 have the same MAR_{PE} of 2:3 and different MIR_{PC} of 3:1, 5:1, 7:1 and 10:1. That of Group No.2 has the same MIR_{PC} of 5:1 and different MAR_{PE} of 1:2, 1:3 and 3:2. It can be found that the value of the output voltage threshold of the SANG is the largest when MIR_{PC} is 3:1 and MAR_{PE} is 2:3. We speculate that the bending degree of the device that the matching ratio of PDMS is 3:1 of Group No.1 is the largest, so that the process of contact-separation is more sufficient, which makes the device more sensitive to the

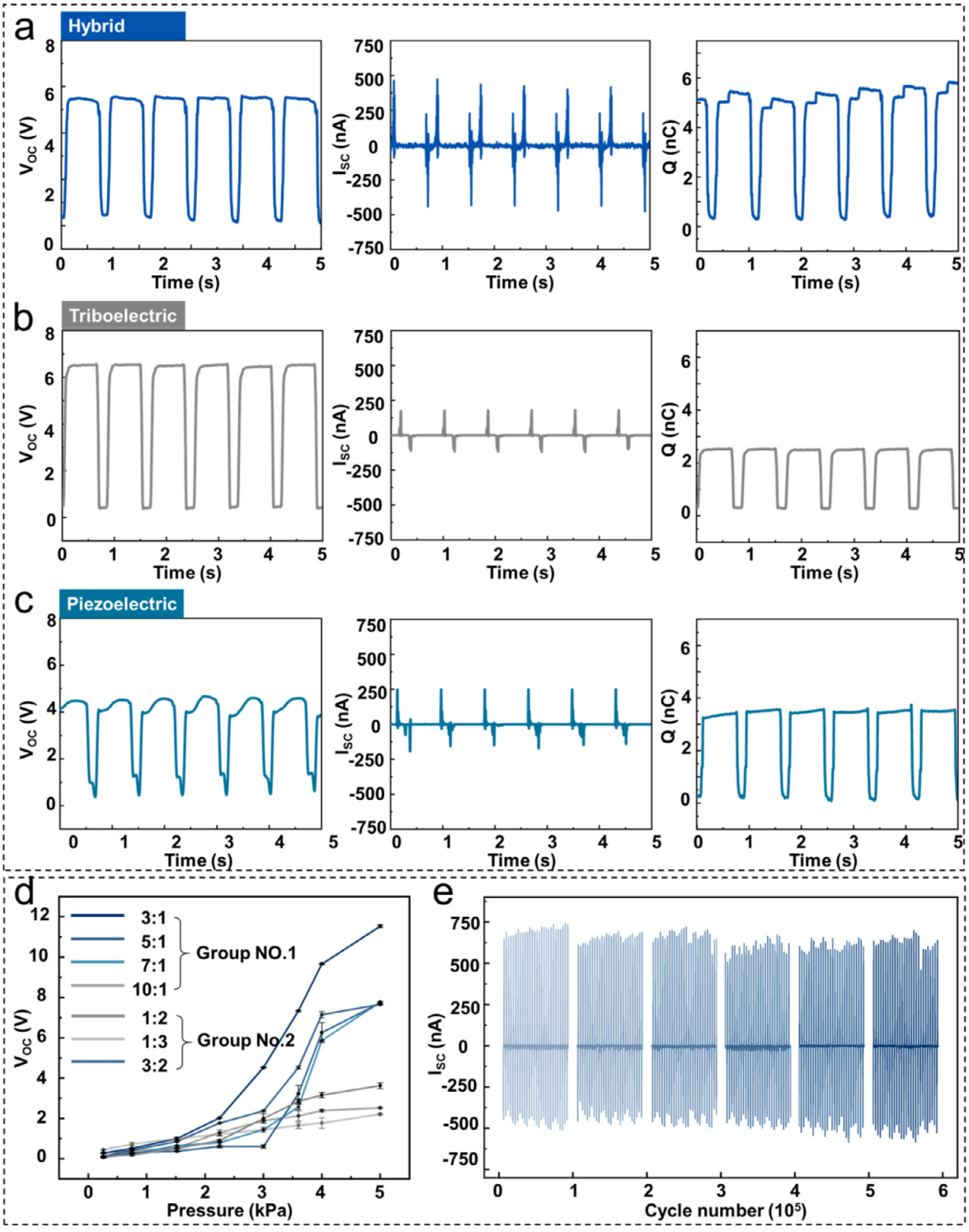

Fig. 4. (a) Outputs of hybrid part of SANG. (b) Outputs of triboelectric part of SANG. (c) Outputs of piezoelectric part of SANG. (d) Outputs of SANGs with different morphologies of self-arched structures under different applied external force. (e) Durability test of the SANG under 10 kPa applied external force with frequency of 2 Hz.

perception of force. In this range, the output voltages have a favorable response to the pressures. As shown in Fig.4e, the mechanical durability of the SANG is characterized by a linear motor providing periodic force to press the SANG for 6×10^5 cycles. There is no significant attenuation of the outputs during and after the mechanical durability test. High-sensitive sensors are usually affected by the overload of external mechanical force while the output of SANG is not affected obviously.

3.4. Application of SANG in pulse sensing

To prove the SANG is suitable for pulse sensing, the device is attached to the wrist for detecting pulse signals (Fig. 5a). Due to the self-arched structure of the polymer composite, the SANG can be deformed effectively and stably when detecting blood vessel movements. Furthermore, the hybrid effect of piezoelectric and triboelectric makes the outputs of the SANG more sensitive. The force

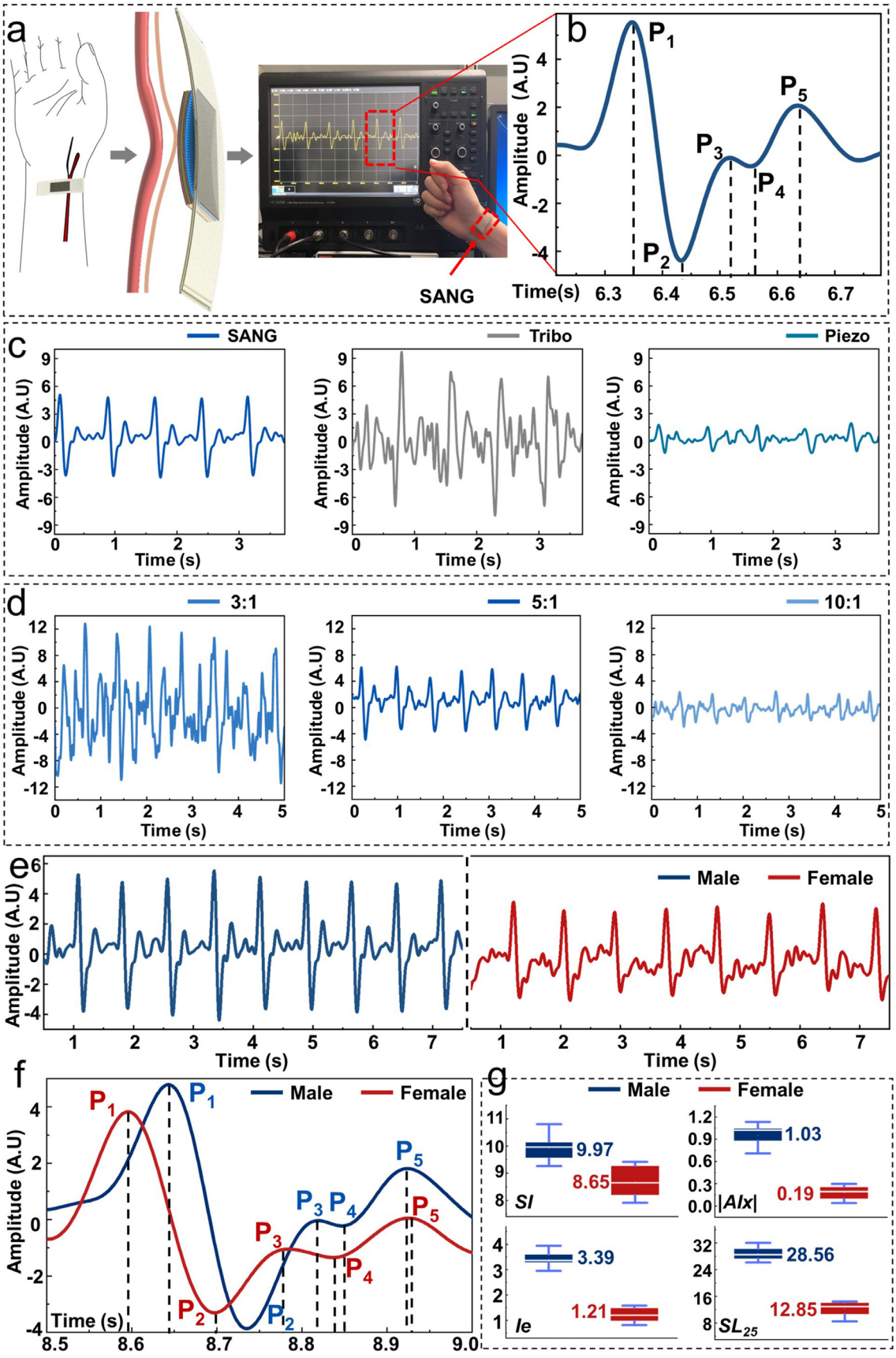

Fig. 5. (a) Pulse waveform of radial artery detected by the SANG. (b) Single cycle pulse waveform. (c) Output properties of three different modes of SANG. (d) Output properties of SANG with different bending degree when detecting pulse signals. (e) Pulse waveform of male and female experimenters. (f) Comparison of single cycle pulse waveform of male and female experimenters. (g) Characteristic parameters of the pulse signals of male and female experimenters.

generates when the pulse beats that give rise to contact and separate between the Ecoflex film and the Al layer of the self-arched structure and the deformation of the PVDF of the SANG. Consequently, the pulse signal is converted to the electrical signal that can reflect the characteristics of human physiology. The output electrical signal is normalized and expressed in terms of amplitude for better observation and comparison, and the unit of amplitude is customized as A.U. The amplitude is directly related to the open-circuit voltage of the device, with a proportional relationship.

The peaks of physiological signals are marked as P_1, P_2, P_3, P_4, P_5 (Fig. 5b), which contain vital physiological and health information such as arterial stiffness, the rhythm of the heart and risk of cardiovascular disease [48,49]. Fig. 5c shows the results of pulse signals tested by the piezoelectric part, the triboelectric part and the hybrid part of SANG, respectively. It is observed that the outputs of the piezoelectric part and the triboelectric part are unstable with some stray peaks caused by noises. In comparison, the outputs of the hybrid part of the SANG are more stable and have better signal-to-noise rates, due to the superposition of the triboelectric and piezoelectric effects [50,51]. The coupling of the triboelectric effect and the piezoelectric effect will fully complement each other's needs for insufficient stress or strain, thereby maximizing the response to the slight pulse and obtaining a clearer and more stable pulse signal. More explanation about the mechanism of the coupling effect of the triboelectrification and the piezoelectricity for a SANG can be found in Supplementary Note 3. Fig. 5d shows the outputs of three groups of the SANGs with the MAR_{PE} of 2:3 and MIR_{PC} of 3:1, 5:1, 10:1, respectively. When the MIR_{PC} is 5:1, the outputs are clearest to reflect the details of the pulse signals. The amplitude of the outputs of the device with the MIR_{PC} of 3:1 is sharp but the noise is too large. Although the noise of the outputs of the SANG with MIR_{PC} of 10:1 is acceptable, the amplitude of the outputs is too small to be detected conveniently. Fig. 5f shows a contrast of the pulse signals between male and female experimenters in the age of twenties.

More details about the pulse waveform of the radial artery have been studied (Fig. 5g). The index of large stiffness (*SI*) and the aortic augmentation index (*AIx*) have a strong relationship with arterial stiffness, which can be used for arterial stiffness diagnosis.

$$SI = \frac{H}{\Delta T} \tag{3}$$

$$AIx = \frac{A(P_2) - A(P_3) - A(P_4) - A(P_5)}{A(P_1)} \tag{4}$$

where H is the height of the experimenter. The time delay between P_1 and P_3 is $\Delta T = T(P_3) - T(P_1)$. $A(P_n)$ is the amplitude of peaks of the pulse waves (P_n, n=1, 2, 3, 4, 5). The *SI* average values of male and female are 9.97 and 8.65, respectively. Moreover, that of $|AIx|$ are 1.03 and 0.19, respectively. According to our previous work [52], another two parameters that *Ie* and SL_{25} are also provided to reflect the arterial conditions further.

$$Ie = A(P_4) - A(P_2) \tag{5}$$

$$SL_{25} = \frac{A(P_5) - A(P_2)}{T(P_5) - T(P_2)} \tag{6}$$

Ie is an index to evaluate the left ventricle ejection capacity. SL_{25} is an indicator of arterial elasticity. The *Ie* average values of the male of the female are 3.39 and 1.21, respectively. And that of SL_{25} are 28.56 and 12.85, respectively. The values of these four parameters of the male are higher than those of the female. It has been reported that gender can affect the pulse waveform of radial artery [53–55]. The data acquired by the SANG show the differences in the waveform signals between males and females. The SANG with an interesting structure might have the potential to be used as a physiological sensor or detecting some other tiny mechanical signals.

4. Conclusions

In summary, the SANG is a spacer-free hybrid nanogenerator with a self-arched structure based on the effect of stress mismatch existing at the interface between two polymers. The morphology of the self-arched structure can be tuned by the mass ratio of PDMS and Ecoflex. With different mass ratios, the bending degrees of the self-arched structure of the SANG are different. More PDMS in the self-arched structure may cause a larger bending degree of it. To get better outputs of the devices, a hybrid mode that combines triboelectric and piezoelectric effects is introduced in the SANG. A thin PVDF film is added into the arched layer to act as a piezoelectric nanogenerator. The peak values of the open-circuit voltage and the short-circuit current of the SANG are 5.2 V and 500 nA. It can be found that the hybrid signal of the SANG is more clear and stable than that of the triboelectric and piezoelectric parts. The SANG has considerable sensitivity and stability to act as a proper device for sensing pulse waveform of the radial artery. The SANG with an interesting structure provides a convenient approach to fabricate physiological sensors, especially to detect micromechanical signals.

5. Auhtor contributions

Y.Z. and J.W.L. conceived the idea and designed the experiment. Z.Li, L.Z., B.J.S. and Y.B.F. guided the project. Y.Z. and J.W.L. designed and fabricated the SANG. C.C.Z. and Z.L. performed the material characterization. Y.Z., J.W.L. and H.Y.O. carried out the related electrical characterization. J.W.L., D.J.J., Z.Liu., and X.C.Q. carried out the physiological signal test. Y.Z. and H.Y.O. analyzed the experimental data. D.J.J., Y.Z. and J.W.L. drew the figures. Y.Z., J.W.L. and B.J.S. prepared the manuscript. All authors discussed and reviewed the manuscript.

Declaration of Competing Interest

All authors declare no conflict of interest of this manuscript.

Acknowledgments

This study was supported by the National Key R&D project from Minister of Science and Technology, China (2016YFA0202703, 2016YFC1102202), National Natural Science Foundation of China (61875015, 11421202 and 11827803), the Beijing Natural Science Foundation (7204275), Science and Technology Commission of Shanghai Municipality (No.17020501000), the Program for Professor of Special Appointment (Eastern Scholar) at Shanghai Institutions of Higher Learning, the University of Chinese Academy of Sciences and the National Youth Talent Support Program.

Supplementary materials

Supplementary material associated with this article can be found, in the online version, at doi:10.1016/j.apmt.2020.100699.

References

[1] S. Niu, et al., Nat. Electron. 2 (8) (2019) 361–368, doi:10.1038/s41928-019-0286-2.
[2] N. Luo, et al., Adv. Mater. Technol. 3 (1) (2018) 1700222, doi:10.1002/admt.201700222.
[3] T.P. Huynh, H. Haick, Adv. Mater. 30 (50) (2018) 1802337, doi:10.1002/adma.201802337.
[4] Y. Gao, et al., Adv. Mater. 32 (15) (2020) 1902133, doi:10.1002/adma.201902133.
[5] C. Wang, et al., Nat. Biomed. Eng. 2 (9) (2018) 687–695, doi:10.1038/s41551-018-0287-x.

[6] L.C. Tai, et al., Adv. Mater. 30 (23) (2018) 1707442, doi:10.1002/adma.201707442.
[7] T.R. Ray, et al., Chem. Rev. 119 (8) (2019) 5461–5533, doi:10.1021/acs.chemrev.8b00573.
[8] J. Kim, et al., Nat. Biotechnol. 37 (4) (2019) 389–406, doi:10.1038/s41587-019-0045-y.
[9] B. Shi, et al., ACS Nano 13 (5) (2019) 6017–6024, doi:10.1021/acsnano.9b02233.
[10] Z. Liu, et al., Adv. Funct. Mater. 29 (20) (2019) 1808820, doi:10.1002/adfm.201808820.
[11] M. Wang, et al., ACS Nano 12 (6) (2018) 6156–6162, doi:10.1021/acsnano.8b02562.
[12] M. Zhu, et al., ACS Nano 13 (2) (2019) 1940–1952, doi:10.1021/acsnano.8b08329.
[13] Y. Zou, et al., Nat. Commun. 10 (1) (2019) 2695, doi:10.1038/s41467-019-10433-4.
[14] M. Wu, et al., Nano Energy 56 (2019) 693–699, doi:10.1016/j.nanoen.2018.12.003.
[15] H. Liu, et al., Appl. Phys. Rev. 5 (4) (2018) 041306, doi:10.1063/1.5074184.
[16] R.A. Surmenev, et al., Nano Energy 62 (2019) 475–506, doi:10.1016/j.nanoen.2019.04.090.
[17] Z.L. Wang, J. Song, Science 312 (5771) (2006) 242–246, doi:10.1126/science.1124005.
[18] Y. Chen, et al., Appl. Catal. B 258 (2019) 118024, doi:10.1016/j.apcatb.2019.118024.
[19] G. Cheng, et al., Adv. Energy Mater. 5 (5) (2015) 1401452, doi:10.1002/aenm.201401452.
[20] R. Hinchet, et al., Science 365 (6452) (2019) 491–494, doi:10.1126/science.aan3997.
[21] F.-R. Fan, et al., Nano Energy 1 (2) (2012) 328–334, doi:10.1016/j.nanoen.2012.01.004.
[22] Y. Qin, et al., Nature 451 (7180) (2008) 809–813, doi:10.1038/nature06601.
[23] X. Chen, et al., Mater. Today 20 (9) (2017) 501–506, doi:10.1016/j.mattod.2017.08.027.
[24] D.Y. Park, et al., Adv. Mater. 29 (37) (2017) 1702308, doi:10.1002/adma.201702308.
[25] Y. Feng, et al., Nano Energy 40 (2017) 481–486, doi:10.1016/j.nanoen.2017.08.058.
[26] C. Sun, et al., Energy Environ. Sci. 4 (11) (2011) 4508–4512, doi:10.1039/C1EE02241E.
[27] Y. Song, et al., Nano Energy 55 (2019) 29–36, doi:10.1016/j.nanoen.2018.10.045.
[28] Q. Zhang, et al., Nano Energy 55 (2019) 151–163, doi:10.1016/j.nanoen.2018.10.078.
[29] H. Ouyang, et al., Nat. Commun. 10 (1) (2019) 1821, doi:10.1038/s41467-019-09851-1.
[30] B. Shi, et al., Adv. Mater. 30 (44) (2018) 1801511, doi:10.1002/adma.201801511.
[31] Y. Feng, et al., ACS Nano 11 (12) (2017) 12411–12418, doi:10.1021/acsnano.7b06451.
[32] Z.L. Wang, Mater. Today 20 (2) (2017) 74–82, doi:10.1016/j.mattod.2016.12.001.
[33] X. Zhang, et al., Nano Energy 4 (2014) 123–131, doi:10.1016/j.nanoen.2013.12.016.
[34] Y. Zheng, et al., Nanoscale 6 (14) (2014) 7842–7846, doi:10.1039/C4NR01934B.
[35] K.Y. Lee, et al., Adv. Energy Mater. 6 (11) (2016) 1502566, doi:10.1002/aenm.201502566.
[36] X. Pu, et al., Sci. Adv. 3 (7) (2017) e1700694, doi:10.1126/sciadv.1700694.
[37] Q. Zheng, et al., Adv. Sci. 4 (7) (2017) 1700029, doi:10.1002/advs.201700029.
[38] T.-I. Lee, et al., Polym. Test. 51 (2016) 181–189, doi:10.1016/j.polymertesting.2016.03.014.
[39] Y.M. Bai, et al., Mater. Sci. Forum 704 (2012) 1284–1290, doi:10.4028/www.scientific.net/MSF.704-705.1284.
[40] J. Bai, et al., J. Am. Ceram. Soc. 90 (1) (2007) 170–176, doi:10.1111/j.1551-2916.2006.01354.x.
[41] T.W. Clyne, in: Key Engineering Materials, 116, Trans Tech Publications Ltd, 1996, pp. 307–330, doi:10.4028/www.scientific.net/KEM.116-117.307.
[42] D.W. Radford, J. Compos. Technol. Res. 15 (4) (1993) 290–296, doi:10.1520/CTR10381J.
[43] G. Twigg, A. Poursartip, G. Fernlund, Compos. Sci. Technol. 63 (13) (2003) 1985–2002, doi:10.1016/S0266-3538(03)00172-6.
[44] K.D. Potter, et al., Compos. Part A 36 (2) (2005) 301–308, doi:10.1016/j.compositesa.2004.06.002.
[45] M.R. Wisnom, et al., Compos. Part A 37 (4) (2006) 522–529, doi:10.1016/j.compositesa.2005.05.019.
[46] Q. Zheng, et al., Adv. Mater. 26 (33) (2014) 5851–5856, doi:10.1002/adma.201402064.
[47] I.-W. Tcho, et al., Nano Energy 42 (2017) 34–42, doi:10.1016/j.nanoen.2017.10.037Get rights and content.
[48] J. Filipovský, et al., Blood Press. 14 (1) (2005) 45–52, doi:10.1080/08037050510008814.
[49] M.R. Nelson, et al., Mayo Clin. Proc. 85 (5) (2010) 460–472, doi:10.4065/mcp.2009.0336.
[50] M. Han, et al., Adv. Electron. Mater. 1 (10) (2015) 1500187, doi:10.1002/aelm.201500187.
[51] B. Shi, et al., Adv. Mater. 28 (5) (2016) 846–852, doi:10.1002/adma.201503356.
[52] H. Ouyang, et al., Adv. Mater. 29 (40) (2017) 1703456, doi:10.1002/adma.201703456.
[53] G. Schwartz, et al., Nat. Commun. 4 (2013) 1859, doi:10.1038/ncomms2832.
[54] A.M. Dart, B.A. Kingwell, J. Am. Coll. Cardiol. 37 (4) (2001) 975–984, doi:10.1016/S0735-1097(01)01108-1.
[55] E. Libhaber, et al., J. Hypertens. 26 (8) (2008) 1619–1628, doi:10.1097/HJH.0b013e328302ca27.